Photoacoustics 15 (2019) 100140

Contents lists available at ScienceDirect

Photoacoustics

journal homepage: www.elsevier.com/locate/pacs

Research article

# Unmixing multi-spectral photoacoustic sources in human carotid plaques using non-negative independent component analysis

M.U. Arabul[a], M.C.M. Rutten[a], P. Bruneval[b], M.R.H.M. van Sambeek[a,c], F.N. van de Vosse[a], R.G.P. Lopata[a,*]

[a] Biomedical Engineering, Eindhoven University of Technology, 5612 AJ Eindhoven, The Netherlands
[b] Service d'Anatomie Pathologique, Hôpital Européen Georges Pompidou, 20 rue Leblanc, 75015 Paris, France
[c] Vascular Surgery, Catharina Hospital Eindhoven, 5623 EJ Eindhoven, The Netherlands

ARTICLE INFO

*Keywords:*
Photoacoustic imaging
Blind unmixing
Independent component analysis
Atherosclerosis
Vulnerable plaques
Morphology
Histology

ABSTRACT

Multi-spectral photoacoustic imaging (MSPAI) is promising for morphology assessment of carotid plaques; however, obtaining unique spectral characteristics of chromophores is cumbersome. We used MSPAI and non-negative independent component analysis (ICA) to unmix distinct signal sources in human carotid plaques blindly. The feasibility of the method was demonstrated on a plaque phantom with hemorrhage and cholesterol inclusions, and plaque endarterectomy samples *ex vivo*. Furthermore, the results were verified with histology using Masson's trichrome staining. Results showed that ICA could separate recent hemorrhages from old hemorrhages. Additionally, the signatures of cholesterol inclusion were also captured for the phantom experiment. Artifacts were successfully removed from signal sources. Histologic examinations showed high resemblance with the unmixed components and confirmed the morphologic distinction between recent and mature hemorrhages. In future pre-clinical studies, unmixing could be used for morphology assessment of intact human plaque samples.

## 1. Introduction

Tissue specificity of photoacoustic imaging (PAI) has sparked research interests in various fields of biomedical imaging and applications [1]. In case tissues have different optical properties (i.e., wavelength-dependent absorption), PAI is able to provide the tissue composition together with the anatomical reference obtained from ultrasound (US). Cardiovascular disease diagnosis is one of the promising areas where PAI has potential in both noninvasive [2–4], and intravascular imaging [5–8]. One important application is the use of PAI to obtain the morphology of atherosclerotic plaques. Using multiple wavelengths, PAI has the potential to reveal the tissue 'signatures' of an unstable plaque such as intraplaque hemorrhages, necrotic lipid pool, and macrophage dispositions [9]. Mostly, the recorded photoacoustic (PA) signals from a plaque are not originating from a single chromophore. Instead, the PA response is the collective contribution of different chromophores. The composition of atherosclerosis is rather complex and different constituents are regarded as a continuum. Recent studies reported that the composition of a plaque is continuously transforming [10]. Findings implied that intraplaque hemorrhages entail the lipid accumulation and that the content of hemorrhages was accompanied mostly by lipids. Therefore, it is not trivial to draw borders between different tissue components at any time in the progression of the plaque. Furthermore, in the literature, it was reported that the PA response of a mixture of components is highly dependent on the concentration of the absorbers [11,12].

Despite the complexity of the tissue composition, the intrinsic chromophores can be revealed using spectral unmixing techniques. In the case the spectrum of the components is exactly known, a linear least-squared error minimization fitting procedure can be used to unmix these sources [13,14]. However, the absorption curve of the chromophores should be known *a priori*, which is not possible for *in vivo* applications. Additionally, this unmixing approach requires higher sampling in the optical spectrum; i.e., the number of wavelengths used in PA measurements should be sufficiently high to fit data accurately. Mercep et al. reported that the number of wavelengths used should be roughly 7 for separating oxygenated and deoxygenated hemoglobin [4]. Finally, wavelength-dependent optical fluence differences should be corrected for in order to make a correct quantitative estimate in linear fitting-based unmixing methods [15,16]. Spectral absorption *in vivo* will be most likely unknown due to the unknown and complex plaque morphology and the reported intersubject variability of optical

* Corresponding author.
*E-mail address:* r.lopata@tue.nl (R.G.P. Lopata).

https://doi.org/10.1016/j.pacs.2019.100140
Received 25 July 2018; Received in revised form 21 May 2019; Accepted 24 June 2019
Available online 25 July 2019

properties [17–19]. Therefore, blind source separation could be an option for PAI of plaques.

In literature, there are studies that classify the PA signals originating from different sources based on signal analysis in the frequency domain [20,21]. The term spectral analysis in those studies refers to the photoacoustic signal frequencies and should not be mistaken with the optical spectrum we are referring to in our study.

In this study, we aimed to adopt a data-driven approach to differentiate distinct components in human carotid plaque samples that have independent spectral behavior under different illumination wavelengths. Therefore, no prior spectral information is required as opposed to fitting based methods. The most commonly used blind unmixing techniques are principal component analysis (PCA) and independent component analysis (ICA). Glatz et al. reported that ICA outperforms PCA in unmixing of PA signals [14,22] by in the sense of better separation. Additionally, PCA can be used complementary to ICA to enhance the unmixing performance as a whole [23]. The classical ICA method assumes a non-Gaussian, zero-mean data distribution of the signal values [24]. However, in the reconstructed PA images, the contrast is based on the optical absorption of different tissues, which yields all positive data. In literature, it was shown that a positivity constraint could improve the performance of linear inversion and unmixing algorithms [25,26]. Therefore, in this study, we used a modified version of the ICA algorithm for non-negative signal sources [27,28].

Furthermore, we used spatially compounded photoacoustic data for unmixing. Due to the rotation of the sample in the spatial compounding, the illumination on the sample is homogenized independent of the acquisition angle (see [29]). The scattering of light in water, which is the surrounding medium for the *ex vivo* experiments, is negligible. Moreover, due to the small size of the sample (wall thickness of 1-5 mm), the optical attenuation was neglected. As a result, the optical fluence over the sample can be assumed to be homogeneous, and no additional fluence correction was performed. For verification of the method, we applied the technique to a plaque phantom made of polyvinyl alcohol (PVA) with three different inclusions: fresh porcine blood, thrombus, and pure cholesterol. Next, for the proof of concept, we applied the technique to human carotid plaque samples ex vivo. We aimed to relate the unmixed components to the critical composition materials that can be found in the plaque. Finally, we performed histologic staining and microscopic examination of stained carotid plaque sections to verify the results of unmixing.

## 2. Materials and methods

### 2.1. Blind source spectral unmixing

Since no prior information regarding the absorption spectrum exists due to the complex plaque morphology, and multiple chromophores concurrently contribute to PA generation, a blind-source unmixing technique was implemented, and its ability to distinguish chromophores in plaque tissue was investigated. Assuming that the contribution of each chromophore to the PA signal is statistically independent [24], the sources can be unmixed with independent component analysis (ICA)[14,22,30]. In this study, the algorithm of Oja et al. for non-negative signal sources was adopted [27,28].

The value of each pixel in a PA image is assumed to be the weighted sum of different PA sources. Then, the PA measurements can be formulated as

$$\overset{p}{\sim} = \mathbf{A}\overset{s}{\sim} \tag{1}$$

where $\mathbf{A}$ is an $m$ by $n$ matrix. The elements of vector $\overset{s}{\sim}$ ($s_j$ for $j$ = 1, 2, 3, …, $n$) represent the actual independent sources and the elements of the matrix $\mathbf{A}$ ($a_{ij}$ for $i$ = 1, 2, 3, …, $m$ and $j$ = 1, 2, 3, …, $n$) represent the weight of the $j$th independent component (IC) for the $i$th measurement. Then, $\overset{p}{\sim}$ becomes a column vector that represents $m$ measurements of a single pixel. Therefore, 2-D PA images were reshaped into a 1-D row vector to treat images as a random variable. Next, PA images from different transverse positions were concatenated to obtain photoacoustic measurement matrix $\mathbf{P}$ of size $m$ by $l$ with $l$ being the total number of pixels.

The number of measurements should be at least equal to the number of independent components for unmixing to converge and lead to an accurate solution. In the case of $m = n$, $\mathbf{A}$ becomes an orthogonal unit variance matrix, i.e., $\mathbf{AA}^T = \mathbf{I}$. Thus, the blind source separation problem can be restated as finding an orthogonal unmixing matrix $\mathbf{U}$ of size $m$ by $m$ from the measurements $\mathbf{P}$ such that

$$\mathbf{Y} = \mathbf{UP} \tag{2}$$

where $\mathbf{Y}$ represents the permutation of independent sources, i.e., different PA absorbers. Unmixing matrix $\mathbf{U}$ was calculated based on an iterative optimization algorithm as described by Oja and Plumbley [27]. First, all PA images from all the plaques were rearranged, so that each row represents a measurement with one of the four wavelengths ($\lambda$ = 808, 915, 940, 980 nm) and columns represent different pixels. Next, data are pre-whitened using an $m$ by $m$ matrix $\mathbf{V}$ to obtain a unit-variance matrix $\mathbf{Z} = \mathbf{VP}$; i.e. the covariance matrix $cov(\mathbf{Z}) = \mathrm{E}((\mathbf{Z} - \mathrm{E}(\mathbf{Z}))(\mathbf{Z} - \mathrm{E}(\mathbf{Z}))^T) = \mathbf{I}$. This is required for working around the zero-mean data distribution requirement of conventional ICA. Finally, an optimization algorithm was applied to the whitened data $\mathbf{Z}$ to find $\mathbf{W}$ such that $\mathbf{Y} = \mathbf{WZ}$, by minimizing the cost function:

$$\mathrm{E}\ \|\mathbf{Z} - \mathbf{W}^T(\mathbf{Y}^+)\|^2. \tag{3}$$

The matrix $\mathbf{Y}^+$ is obtained by selecting only the positive values of $\mathbf{Y}$. See the study by Oja and Plumbley [27] for further details of the algorithm.

The unmixing algorithm was applied to the datasets of individual plaque samples both separately, and to a combined dataset, i.e., all plaque PAI datasets merged as input for one unmixing step.

### 2.2. Sample preparation for imaging

#### 2.2.1. PVA phantom preparation

A simplified plaque phantom was made to investigate the unmixing of different tissue components concurrently. The phantom is a cylindrical vessel tube of polyvinyl alcohol (PVA) with an external diameter of 8 mm and an internal diameter of 3 mm. Additionally, the mold was designed such that three cylindrical holes of 1 mm diameter in the vessel wall were available for inclusion materials (see Fig. 1). The PVA gel was prepared in demi-water with 15 wt% PVA (Mowiol 28-99, Sigma–Aldrich, Zwijndrecht, The Netherlands), and 1 wt% Orgasol (ELF Atochem, Paris, France) as acoustic scatterers to mimick Rayleigh scattering of biological tissue [29]. Next, the gel was injected into the mold and subjected to 2 freeze-thaw cycles, i.e., freezing for 16 h and thawing for 8 h to stiffen the cryogel. Finally, the three inclusions were injected into the holes in the vessel wall, and the open ends were sealed

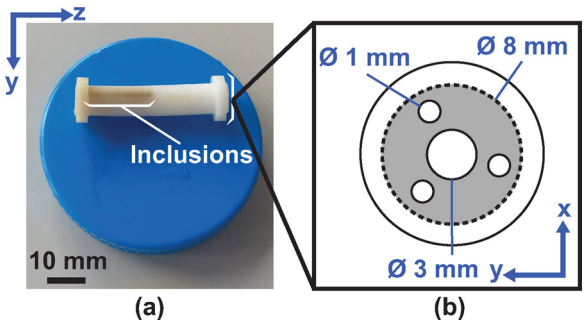


**Fig. 1.** (a) The polyvinyl alcohol vessel phantom. (b) Illustrations of the phantom including dimensions. The diameter of the ends of the cylinder were enlarged for easy attachment to the imaging setup. The dashed-line indicates the diameter in the vessel area.

using PVA and one additional freeze-thaw cycle. Porcine blood, freshly obtained from a local slaughterhouse, was used to mimic recent intraplaque hemorrhages. Next, human thrombus, obtained as waste material from an abdominal aortic aneurysm surgery, was used to mimic aged hemorrhages. Since the absorption spectrum of hemoglobin varies with chemical interaction of it with other compounds, an alteration of the absorption was expected due to the transformation from hemoglobin to methemoglobin in aged hemorrhages [31]. Finally, commercially available cholesterol crystals (C8667, Sigma–Aldrich Chemie GmbH, Munich, Germany) were added to the third channel, representing a lipid inclusion [32].

#### 2.2.2. Human plaque samples

The carotid plaques were excised during carotid endarterectomy operations at the Catharina Hospital Eindhoven and transferred to the photoacoustic laboratory. The study was approved by the local ethics committee, and the samples were collected with the informed consent of the patients. Once the intact plaque sample was obtained, it was flushed with a phosphate-buffered-saline (PBS) solution to remove excess blood from the outer surface and the lumen. Next, two plastic cannulas were glued to the tips of the sample so that it could be mounted to the rotational measurement setup [33,29]. In case the measurements were not performed on the day of the surgery, the samples were snap-frozen in liquid nitrogen and conserved at −80 °C until the experiment, and defrosted at room temperature prior to the PA measurements.

### 2.3. Scanning setup and photoacoustic acquisition system

Each sample was scanned in a custom-designed setup that allows controlled positioning ($x$, $y$, $z$) of the PA probe and the angular position ($\theta$) of the sample. The setup consists of an immersion chamber (see Fig. 2), a three-dimensional (3-D) linear stage (M-403.2DG, Physik Instrumente, Germany), and a rotary controller (RS-40 DC, Physik Instrumente, Germany) controlled by a PC using LabVIEW software (National Instruments, Austin, Texas, USA). For a detailed description of the setup, we refer to Arabul et al. 2016 [33].

The PA imaging probe consisted of a diode laser (Lumibird, Paris, France) with four wavelengths ($\lambda$ = 808, 915, 940, 980 nm), capable of generating pulses with a pulse duration of 130 ns and energy of 1 mJ (< 20 mJ/cm$^2$, ANSI Safety Standard). The wavelengths used in this study were chosen in the NIR band (800 nm to 1000 nm) of the optical spectrum to increase the penetration depth of optical energy and considering optical absorption spectrum of the tissue components. The reason of having those four specific discrete wavelengths was dictated by the availability of the diode lasers. The acoustic signals were acquired by a linear array transducer (SL3323, ESAOTE, Maastricht, The Netherlands) that was integrated into the PA probe. For data acquisition, the PA probe was attached to an ultrasound scanner (MyLabOne, ESAOTE, The Netherlands), and the raw data were digitized at a sampling frequency of 50 MHz before transfer to a PC [34]. For a detailed description of the experiment setup and PA probe, we refer to Arabul et al. [33].

### 2.4. Experiment protocol

A single image frame in both PA and US mode is obtained after spatially compounding the image data acquired from 36 different angular positions. The spatial compounding enhances the image quality by reducing the speckle and sharpening the boundaries in the US images (see the lumen and the outer boundary of the PVA phantom in Fig. 1). The details and the advantages of spatial compounding method were presented previously by Arabul et al. [29]. Briefly, the PA probe was positioned to image a cross-section of the sample, and the images were acquired by rotating the sample by 10°, covering the full 360°. Next, the 3-D stage moves to the next transverse position with a step size of 0.5 mm, and the pseudo-tomographic, compound imaging is repeated. Depending on the length of the sample, approximately 50 cross-sectional images were recorded for each wavelength. During the experiment, the temperature of the immersion bath was kept at body temperature (37 °C). The effect of the temperature was not tested; however, it is known from the literature that the PA pressure increases with increasing medium temperature [35,36]. Therefore, body temperature was preferred instead of room temperature.

### 2.5. Histology procedure

The plaque samples were fixated in 3.7% formalin solution for 24 h. Next, the samples were decalcified in buffered ethylenediaminetetraacetic acid (EDTA) solution for a week. The buffered EDTA solution was prepared by mixing 400 ml phosphate buffered saline (PBS) solution with 40 g of ETDA powder (Sigma–Aldrich Chemie GmbH, Munich, Germany). Next, NaOH pellets (Merck, Darmstadt, Germany) were added gradually to adjust the pH to 7.5.

Next, tissue samples were dehydrated with a standard tissue processor (Microm STP 120, Thermo Fisher Scientific, Walldorf, Germany) and embedded in paraffin blocks. Samples were sectioned in the transverse plane with the thickness of 5 µm using a microtome (RM2255, Leica Microsystems B.V., Amsterdam, The Netherlands). Finally, histology sections were stained with Weigner's Iron Hematoxylin and Mason's trichrome (Sigma–Aldrich Chemie GmbH, Munich, Germany). The histology overview images were manually matched to the US images based on the structural similarity of the lumen and vessel wall.

## 3. Results

The results of the plaque phantom are presented in Fig. 3 demonstrating the effect of unmixing on PA data. See Supplementary Fig. A.7 for the effect of unmixing similarly on *ex vivo* plaque data. Fig. 3b is the compounded US image that clearly resembles the geometry of the phantom. The echogenicity is lowest for the blood and the highest for the cholesterol crystal. The high echogenicity of the cholesterol is due to the relatively stiff crystal form of the cholesterol used, and should not be mistaken for calcifications in plaque samples. The PA images of the phantom obtained at the four available wavelengths ($\lambda$ = 808, 915, 940, 980 nm) are shown in Fig. 3c–f. The dynamic range of the

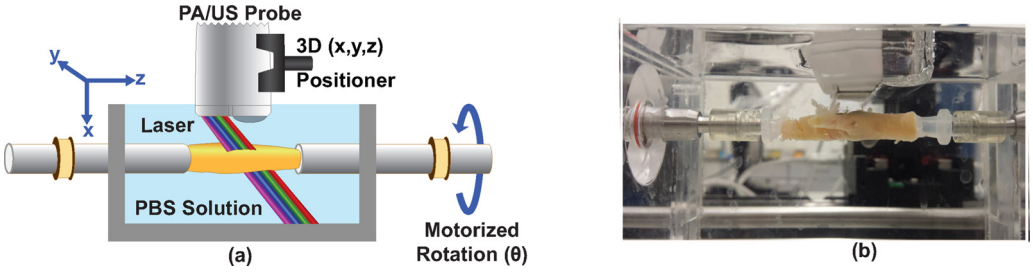


**Fig. 2.** Illustration (a) and picture (b) of the experimental setup and photoacoustic (PA) probe used in this study.

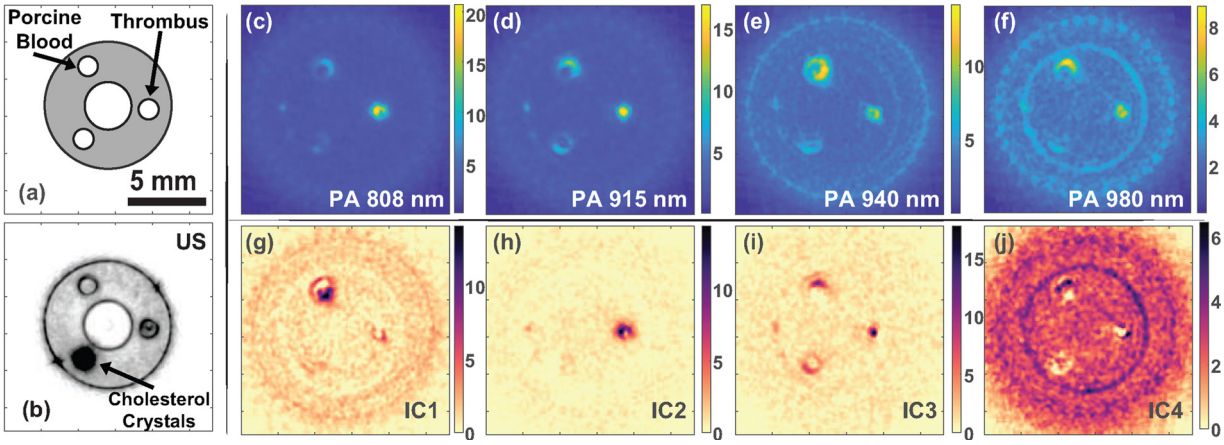


**Fig. 3.** A cross-section image of PVA phantom: (a) an illustration, (b) ultrasound (US) image, (c–f) photoacoustic (PA) measurements at wavelengths λ = 808, 915, 940, 980 nm and (g–j) unmixed independent components, labeled as IC1 to IC4.

colormap of each PA image is normalized with respect to its maximum intensity. Although the signal intensities vary, all four PA images provide signals from all three inclusions. The signals from the cholesterol are much lower than the hemorrhages due to low absorption of lipid in the spectral range available. However, as seen in Fig. 3g–j, the results of blind source unmixing do reveal different patterns of the plaque. The unmixed components are labeled as follows: IC1 is fresh blood, IC2 is the thrombus-based hemorrhage, IC3 shows the signal from all three components, and lastly, IC4 is the compounding artifact with the outer boundary of the sample.

The overlaid US and PA images were rendered in 3-D, see Fig. 4, to provide an overview of all samples and to demonstrate the continuity in the unmixed PA sources through the transverse imaging planes of the samples. However, at this step, unmixed ICs are blind to the actual sources and Fig. 4 is not intended to demonstrate the actual chromophores. For visualization, non-linear transparency functions were used as the alpha channel for each image. Since the unmixing algorithm pushes the histogram of the sources away from each other, a different part of the colormap remains visible for different images after applying transparency in 3-D. Therefore, the different colors does not carry any information regarding type of the actual chromophores. The colors represent the presence of signals of the corresponding ICs.

The unmixing algorithm was applied to each individual carotid plaque dataset, and to a combined dataset, i.e., all plaque PAI datasets were combined and used as input for a single unmixing step. Due to variation in the signal-to-noise ratios (SNR) in the different datasets (see Appendix A.2), unmixing performance decreases when all data were used together; i.e., the optimization converges with a more substantial mean-squared error (MSE). Despite the more noisy output, the converged optima and patterns of unmixed components did not alter significantly. Since the order of the unmixed components is arbitrary, the result of unmixing on combined data was used as a reference to obtain a consistent permutation of the independent components for all samples (i.e., sort them in the same order). The results of unmixing by non-negative ICA was completely blind to the sources and were not based on any assumptions regarding physical sources of PA.

The magnified histologic images were presented in Fig. 6 to verify the match between the ICs and plaque components. In Fig. 5, the results of unmixed PA data are presented together with the histology overview and US images to provide the structural resemblance between US and histology. Each row represents a different cross-section (denoted as S1 and S2) obtained in three plaque samples (P1 to P3). The cross-section labeled as P3S1 is from the bifurcation of the carotid and the internal branch was damaged during the histology. Therefore, only one branch is visible in the histology image, while both branches were present during US and PA measurements. The results of unmixing for plaque cross-sections are in agreement with the phantom results. IC1 represents the recent hemorrhages with a more confined area. IC2 shows a lower signal contrast than IC1; however, the area that provides a signal is generally originating from a larger area. Similar to the results of the phantom, IC4 resembles the outer boundary of the sample and the compounding artifact (circular haze). However, linking IC3 to any actual tissue components is not feasible using only Fig 5 .

Based on the overview of histology pictures, no indication of PA-based lipid detection was observed in the plaque samples, which is in contrast to the case of the pure cholesterol inclusion in the phantom. Therefore, further analysis of the histology images was performed, where the slices were subjected to microscopic examination (see Fig. 6).

More robust evidence of the correspondence between the ICs and the actual chromophores can be obtained examining sub-regions in the histology images more closely. In Fig. 6 the histologic examination of two cross-sections is demonstrated, which supports the findings in the phantom experiments. The presence of erythrocytes (see Fig. 6a–I) is evidence of recent hemorrhages, which matches with the dark high-intensity signals in the IC1 image. For the cross-section P1S1, the presence of erythrocytes is also confirmed in the zoomed image in Fig. 6b–I, which coincides with the signals in IC1 of the same section. Detailed examination of the histology sections for the regions with high signals in IC2 revealed the common morphological characteristics. Having a darker pink color then it's surrounding indicates the existence of matured hemorrhages in the vicinity. Additionally, those regions are accompanied by sharp-edged void areas that resemble the cholesterol clefts (see Fig. 6a–II and b–II). This supports previous literature that old hemorrhages trigger lipid accumulation and their presence is mostly concurrent [10].

Finally, the high signal regions in IC4 coincide with the outer layer of the sample, see Fig. 6(a–III) and (b–III). That is the media layer of the artery; however, we strongly believe that this component is the PA signals generated on the surface of the sample. This is confirmed by the evidence that the same signal component was also present in the PVA phantom experiment. Since that surface PA signal also presents uniform behavior over the spectrum, it remains in the same component as the artifact.

## 4. Discussion

In this study, we showed the feasibility of blind-source spectral unmixing of multi-wavelength PA data obtained in human carotid plaques *ex vivo*. We adopted non-negative independent component analysis (ICA) for unmixing reconstructed optical absorption maps obtained from PA measurements. We showed that unmixed components of PA images show high resemblance with the inclusions in the phantom

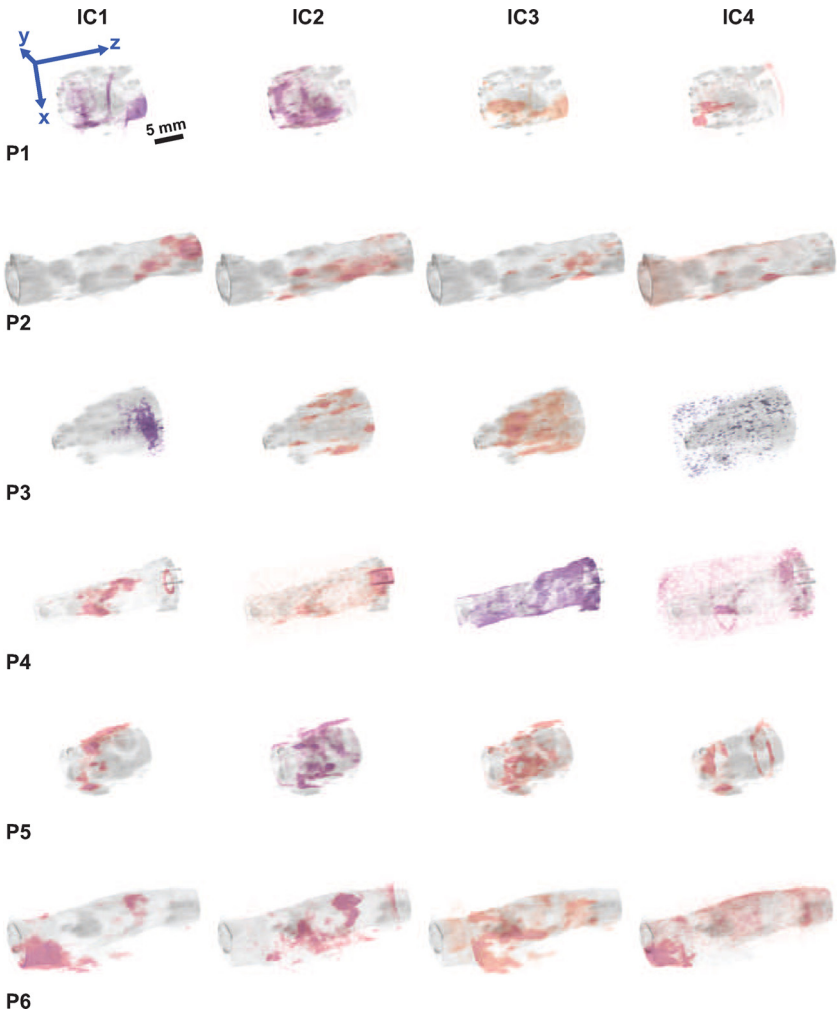


**Fig. 4.** 3-D rendered overlay images of ultrasound (US) and unmixed photoacoustic signals, labeled as independent component (IC) IC1 to IC4. Each row shows a different carotid plaque sample (labeled P1 to P6). The scale bar is representative for all the samples, indicating that the longitudinal size of the plaque samples varies between 1 and 3 cm.

experiments. Furthermore, we demonstrated that the results of unmixed components in distinct regions in the PA images that were corroborated by the histology images.

Based on the ICA theory, the number of measurements should be at least equal to the number of independent components. We used 4 wavelengths in our measurements due to design considerations of our PAI system. Therefore, we wanted to investigate the highest possible independent components without making any assumptions on the number of actual independent components. The number of wavelengths used during measurements would not directly affect the separation performance of ICA, the performance is rather determined by the independency of the components at those wavelengths. Next, we investigated the continuity of the ICs in 3-D space (from cross-section to cross-section), and the resemblance between the ICs and the main components of the plaque tissues using histologic examination. In case there were more ICs than 4, the unmixing may converge to a linear combination of the independent sources, which would not infringe the link between the histologic examinations.

The two dominant PA sources, recent and matured hemorrhages, were successfully discriminated using blind-source unmixing. Detection of intra-plaque hemorrhages is vital to capture indications of plaque vulnerability. Therefore, this can potentially be used to differentiate hemorrhages from the luminal blood when applied to *in vivo* data. Additionally, ICA was able to separate the artifacts from the signal sources. The compounding artifacts have a uniform response over the spectrum, and, therefore, are independent of the actual signal sources. Separating ICs from these background artifact yields denoising of multispectral PA data, which was IC4 in our experiments. For IC3, it was not possible to relate it to any plaque components. In the PVA phantom experiments, IC3 provided signals from all three inclusions, hence not specific to any components. In our phantom, pure cholesterol crystals of one single type were used rather than a mixture as would be found *in vivo* [32,37]. Moreover, the available wavelengths in this study were not optimal for PA signal generation in lipids. Therefore, the unmixing performance of the human plaque samples is expected to be different from the phantom experiments.

Providing a quantitative comparison between PA and histology is not trivial due to the difficulty in the examination of histologic pictures. Even for skilled pathologists it is not trivial to determine the location of morphological features. Therefore, we believe that the limiting factor is not solely the contrast in the IC images but also the complexity of the plaque composition.

The primary advantage of blind source unmixing is that no a priori data on the PA sources is needed, which makes the technique suitable for *in vivo* application. However, at the same time, this also is the main drawback of the technique due to the non-specific order of sources. Using a phantom, we were able to relate the unmixed sources in the plaque samples to the inclusions for proof of principle. Moreover, it provided partial validation of the signals measured in the plaque samples despite the limitations of the phantom as mentioned earlier.

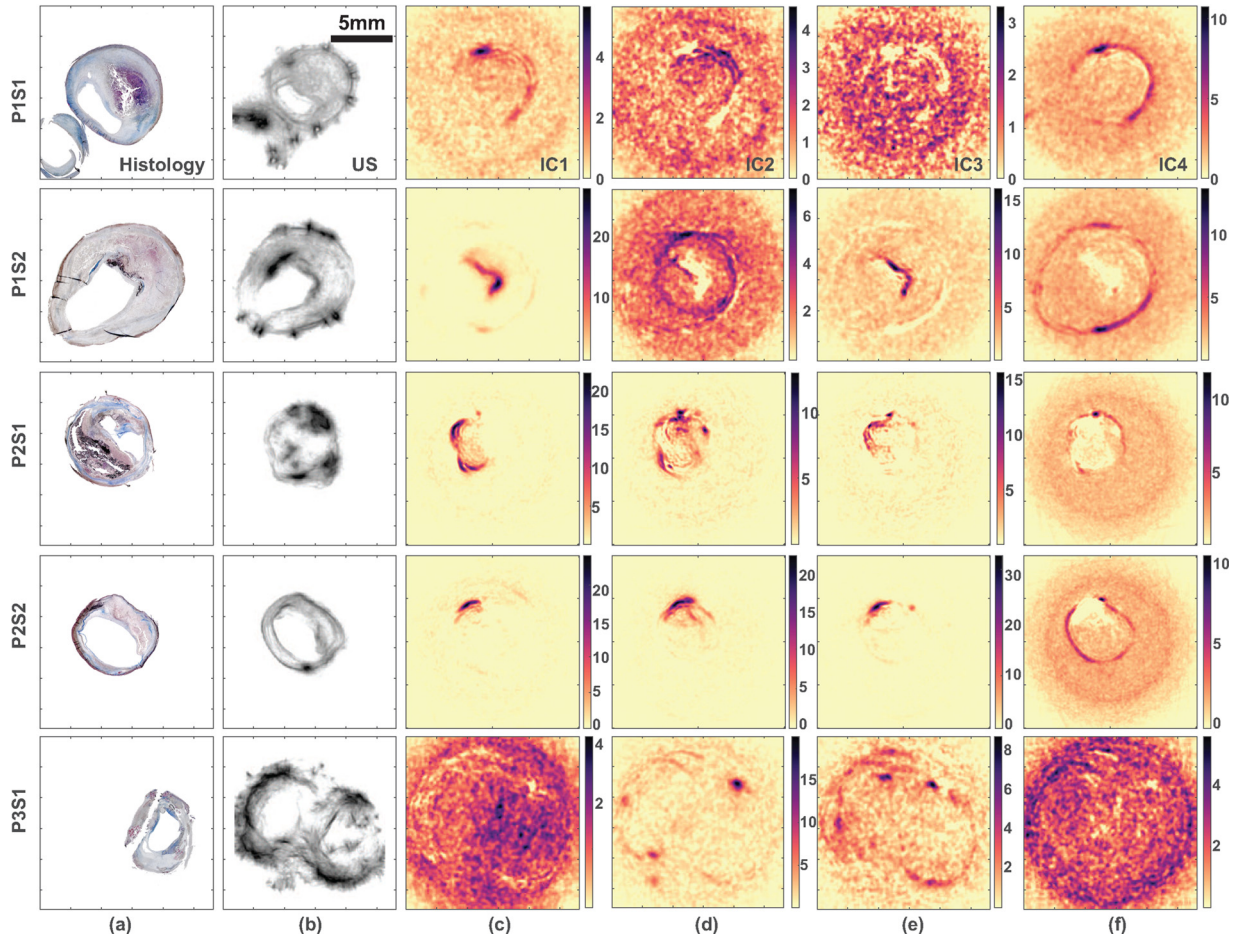


**Fig. 5.** Overview of the measurements from five different cross-sections of three plaque samples and a cross-section of the PVA phantom. Rows show different cross-sections and the annotation P1S1 stands for 'plaque one – section one'. The first column (a) is the histology section corresponding to the measured cross-section. The second column (b) is the US image to show the geometry of the measured cross-section. Please note that the dark color in the US image indicates high echogenicity. The columns from (c) to (f) are the independent components (IC1 – IC4) as the output of the unmixing algorithm. Darker color represents a higher signal in the unmixed source.

The results of ICA yields unmixed components that have a distinct characteristic in the optical absorption spectrum for the measured wavelengths only. Nevertheless, it is possible to infer quantitative absorption values of the chromophores using ICA.

The contrast of the unmixed ICs varies between the cross-sections of different samples. One possible reason for the different contrast levels could be the actual plaque composition in the imaged cross-section. A healthy carotid, for example, almost gives no signal in the wavelengths used as we observed in the healthy sections (the ends of the samples) of the plaque samples. In the results sections, we presented the high contrast results as well as the lower contrast images to demonstrate the overall performance of the unmixing without any bias.

During histology, the tissues were subjected to a sequence of chemical processes, which cause structural deformation. Therefore, the automatic registration of histology images to the images of a different modality, US images, was not feasible. Hence, a first, qualitative comparison of the selected cross-sections to the unmixed PA data was presented instead of a quantitative comparison including all the cross-sections.

Blind-source spectral unmixing using non-negative ICA is promising for prospective *in vivo* application of PAI for carotid plaques. The findings of this study revealed the potential of non-negative ICA for spectral unmixing of multi-wavelength PAI for future clinical studies. However, this work is merely a proof of concept, and *in vivo* measurements in patients are beyond the scope of the current study. Spatial compounding can elevate the image quality when applied *in vivo* [29], whereas ICA-based unmixing can identify different plaque regions and remove the compounding artifact from actual signal sources. The principle of ICA dictates that all the data from different measurements should be complete. Therefore, it can only be implemented for off-line data. However, the mixing matrices obtained from real plaque samples can be used as a lookup table for real-time measurements. Possible unmixed components can be generated based on the same linear mixing model provide insight into the components.

For the future, a larger pre-clinical study is planned to support the findings in this study and showing the clinical relevance for a larger population. Furthermore, to obtain a better tissue specificity, additional staining methods will be used in histology to stain additional materials such as macrophages, collagen, and lipid.

## 5. Conclusion

In conclusion, we showed that a data-driven approach could be used to differentiate chromophores in human carotid plaque samples based on their independent PA response for distinct wavelengths. We used the non-negative ICA algorithm on spatially compounded photoacoustic data and showed that the recent hemorrhages and mature hemorrhages on plaques could be differentiated. Additionally, the signatures of cholesterol clefts were captured, which is supported by the phantom experiment and histologic analysis. Furthermore, using ICA, we demonstrated that the background artifact could be removed in the unmixed components, which elevated the PA image quality of unmixed

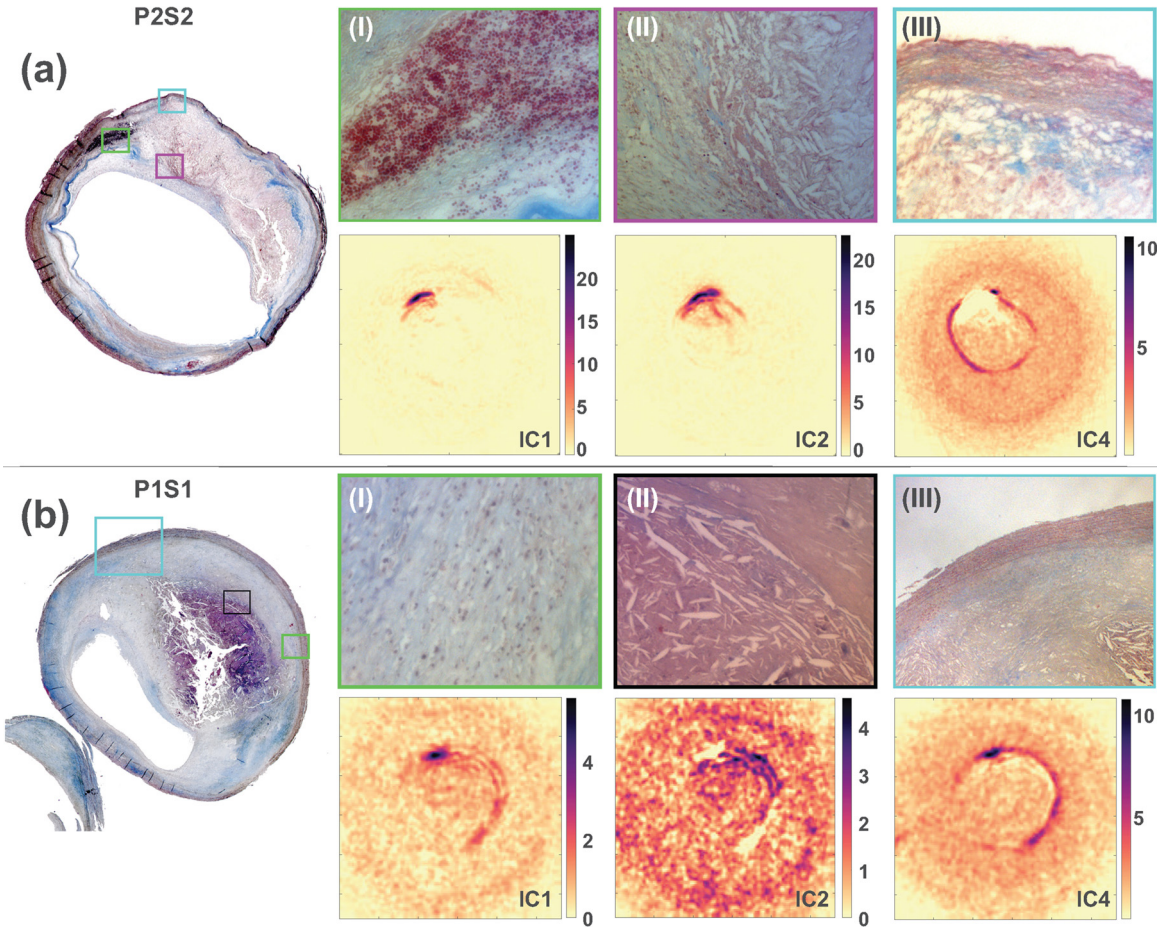


**Fig. 6.** Histological details of plaque sample one – cross-section one (P1S1) and plaque sample two – cross-section two (P2S2). The overview of the histology is shown for two histologic sections in (a) and (b). The images (I) to (III) are the three magnified microscopy images of the histologic section. The locations of the magnified areas are indicated by the rectangles with different frame colors.

components. The results of this study showed the merit of blind-source spectral unmixing for morphological assessment of the complex tissue compositions as carotid plaques, in which the spectral absorption is most likely unknown.

## Acknowledgments

The author acknowledges Hans-Martin Schwab and Georg Schmitz from the Ruhr-Universität Bochum for valuable discussions regarding spectral unmixing. We would also like to show our gratitude to Dr. Aryan Vink from the University Medical Center Utrecht for contributions on histologic examination. This study is funded by the European Community's Horizon2020 (CVENT) under grant agreement no: 731771.

## Appendix A. Supplementary data

Supplementary data associated with this article can be found, in the online version, at https://doi.org/10.1016/j.pacs.2019.100140.

## References

[1] Y. Liu, L. Nie, X. Chen, Photoacoustic molecular imaging: from multiscale biomedical applications towards early-stage theranostics, Trends Biotechnol. 34 (5) (2016) 420–433.
[2] A. Dima, V. Ntziachristos, Non-invasive carotid imaging using optoacoustic tomography, Optics Express 20 (22) (2012) 25044.
[3] P. Kruizinga, A.F.W. van der Steen, N. de Jong, G. Springeling, J.L. Robertus, A. van der Lugt, G. van Soest, Photoacoustic imaging of carotid artery atherosclerosis, J. Biomed. Optics 19 (11) (2014) 110504.
[4] E. Merčep, X.L. Deán-Ben, D. Razansky, Imaging of blood flow and oxygen state with a multi-segment optoacoustic ultrasound array, Photoacoustics 10 (1) (2018) 48–53.
[5] S. Sethuraman, S. Aglyamov, J. Amirian, R. Smalling, S. Emelianov, Intravascular photoacoustic imaging using an IVUS imaging catheter, IEEE Trans. Ultrasonics Ferroelectr. Freq. Control 54 (5) (2007) 978–986.
[6] B. Wang, J.L. Su, A.B. Karpiouk, K.V. Sokolov, R.W. Smalling, S.Y. Emelianov, Intravascular photoacoustic imaging, IEEE J. Sel. Topics Quantum Electron. 16 (3) (2010) 588–599.
[7] A. Rosenthal, F.A. Jaffer, V. Ntziachristos, Intravascular multispectral optoacoustic tomography of atherosclerosis: Prospects and challenges, Imaging Med. 4 (3) (2012) 299–310.
[8] M. Wu, G. Springeling, M. Lovrak, F. Mastik, S. Iskander-Rizk, T. Wang, H.M.M. van Beusekom, A.F.W. van der Steen, G. Van Soest, Real-time volumetric lipid imaging in vivo by intravascular photoacoustics at 20 frames per second, Biomed. Optics Express 8 (2) (2017) 943.
[9] B. Wang, E. Yantsen, T. Larson, A.B. Karpiouk, S. Sethuraman, J.L. Su, K. Sokolov, S.Y. Emelianov, Plasmonic intravascular photoacoustic imaging for detection of macrophages in atherosclerotic plaques, Nano Lett. 9 (6) (2009) 2212–2217.
[10] F.D. Kolodgie, H.K. Gold, A.P. Burke, D.R. Fowler, H.S. Kruth, D.K. Weber, A. Farb, L.J. Guerrero, M. Hayase, R. Kutys, J. Narula, A.V. Finn, R. Virmani, Intraplaque hemorrhage and progression of coronary atheroma, New Engl. J. Med. 349 (24) (2003) 2316–2325.
[11] J. Laufer, D. Delpy, C. Elwell, P. Beard, Quantitative spatially resolved measurement of tissue chromophore concentrations using photoacoustic spectroscopy: application to the measurement of blood oxygenation and haemoglobin concentration, Phys. Med. Biol. 52 (1) (2007) 141–168.
[12] B.T. Cox, J.G. Laufer, P.C. Beard, S.R. Arridge, Quantitative spectroscopic photoacoustic imaging: a review, J. Biomed. Optics 17 (6) (2012) 061202.
[13] N. Keshava, J.F. Mustard, Spectral unmixing, IEEE Signal Process. Mag. 19 (1) (2002) 44–57.
[14] J. Glatz, N.C. Deliolanis, A. Buehler, D. Razansky, V. Ntziachristos, Blind source unmixing in multi-spectral optoacoustic tomography, Optics Express 19 (4) (2011) 3175.
[15] S. Tzoumas, N. Deliolanis, S. Morscher, V. Ntziachristos, Unmixing molecular agents from absorbing tissue in multispectral optoacoustic tomography, IEEE Trans.

Med. Imaging 33 (1) (2014) 48–60.
[16] S. Tzoumas, A. Nunes, I. Olefir, S. Stangl, P. Symvoulidis, S. Glasl, C. Bayer, G. Multhoff, V. Ntziachristos, Eigenspectra optoacoustic tomography achieves quantitative blood oxygenation imaging deep in tissues, Nat. Commun. 7 (1) (2016) 12121.
[17] G.S. Abela (Ed.), Lasers in Cardiovascular Medicine and Surgery: Fundamentals and Techniques, Developments in Cardiovascular Medicine, Springer, US, 1990.
[18] A.J. Welch, M.J.C. van Gemert (Eds.), Optical-Thermal Response of Laser-Irradiated Tissue, 2nd ed., Springer, Netherlands, 2011.
[19] S.L. Jacques, Optical properties of biological tissues: a review, Phys. Med. Biol. 58 (11) (2013) R37–R61.
[20] G. Xu, Z.-X. Meng, J.D. Lin, J. Yuan, P.L. Carson, B. Joshi, X. Wang, The functional pitch of an organ: quantification of tissue texture with photoacoustic spectrum analysis, Radiology 271 (1) (2014) 248–254.
[21] Y. Cao, A. Kole, L. Lan, P. Wang, J. Hui, M. Sturek, J.-X. Cheng, Spectral analysis assisted photoacoustic imaging for lipid composition differentiation, Photoacoustics 7 (2017) 12–19.
[22] L. An, B. Cox, Independent component analysis for unmixing multi-wavelength photoacoustic images, in: A.A. Oraevsky, L.V. Wang (Eds.), Proceedings of SPIE, Vol. 9708 of Proceedings of SPIE, 2016, p. 970851.
[23] X.L. Deán-Ben, A. Buehler, D. Razansky, V. Ntziachristos, Estimation of optoacoustic contrast agent concentration with self-calibration blind logarithmic unmixing, Phys. Med. Biol. 59 (17) (2014) 4785–4797.
[24] A. Hyvärinen, E. Oja, Independent component analysis: algorithms and applications, Neural Netw. 13 (4–5) (2000) 411–430.
[25] L. Ding, X. Luís Deán-Ben, C. Lutzweiler, D. Razansky, V. Ntziachristos, Efficient non-negative constrained model-based inversion in optoacoustic tomography, Phys. Med. Biol. 60 (17) (2015) 6733–6750.
[26] L. Ding, X.L. Deán-Ben, N.C. Burton, R.W. Sobol, V. Ntziachristos, D. Razansky, Constrained inversion and spectral unmixing in multispectral optoacoustic tomography, IEEE Trans. Med. Imaging 36 (8) (2017) 1676–1685.
[27] E. Oja, M. Plumbley, Blind separation of positive sources by globally convergent gradient search, Neural Comput. 16 (9) (2004) 1811–1825.
[28] Z. Yuan, E. Oja, A FastICA Algorithm for Non-Negative Independent Component Analysis vol. 3195, Springer Berlin Heidelberg, 2004.
[29] M.U. Arabul, H.M. Heres, M.C.M. Rutten, M.R.H.M. van Sambeek, F.N. van de Vosse, R.G.P. Lopata, Investigation on the effect of spatial compounding on photoacoustic images of carotid plaques in the in vivo available rotational range, IEEE Trans. Ultrason. Ferroelectr. Freq. Control 65 (3) (2018) 440–447.
[30] S. Morscher, J. Glatz, N.C. Deliolanis, A. Buehler, A. Sarantopoulos, D. Razansky, V. Ntziachristos, Spectral unmixing using component analysis in multispectral optoacoustic tomography, Proc. of SPIE-OSA Biomedical Optics, OSA, 2011, p. p80890.
[31] J. Umbreit, Methemoglobin – it's not just blue: a concise review, Am. J. Hematol. 82 (2) (2007) 134–144.
[32] K. Jansen, M. Wu, A.F.W. van der Steen, G. van Soest, Photoacoustic imaging of human coronary atherosclerosis in two spectral bands, Photoacoustics 2 (1) (2014) 12–20.
[33] M.U. Arabul, M. Heres, M.C.M. Rutten, M.R. van Sambeek, F.N. van de Vosse, R.G.P. Lopata, Toward the detection of intraplaque hemorrhage in carotid artery lesions using photoacoustic imaging, J. Biomed. Optics 22 (4) (2016) 041010.
[34] K. Daoudi, P.J. van den Berg, O. Rabot, A. Kohl, S. Tisserand, P. Brands, W. Steenbergen, Handheld probe integrating laser diode and ultrasound transducer array for ultrasound/photoacoustic dual modality imaging, Optics Express 22 (21) (2014) 26365.
[35] I.V. Larina, K.V. Larin, R.O. Esenaliev, Real-time optoacoustic monitoring of temperature in tissues, J. Phys. D: Appl. Phys. 38 (15) (2005) 2633.
[36] J. Shah, S. Park, S. Aglyamov, T. Larson, L. Ma, K. Sokolov, K. Johnston, T. Milner, S.Y. Emelianov, Photoacoustic imaging and temperature measurement for photothermal cancer therapy, J. Biomed. Optics 13 (3) (2008) 034024.
[37] T. Buma, N.C. Conley, S.W. Choi, Multispectral photoacoustic microscopy of lipids using a pulsed supercontinuum laser, Biomed. Optics Express 9 (1) (2017) 276–288.

M. Umit Arabul received the B.Sc. degree in electrical and electronics engineering from the Middle East Technical University, Ankara, Turkey, and a M.Sc. degree in biomedical engineering from the Institute of Biomedical Engineering, Bogaziçi University, Istanbul, Turkey. He obtained his Ph.D. degree at the Eindhoven University of Technology, Eindhoven, The Netherlands. His research interests include in vivo photoacoustic imaging of carotid arteries and fundamental characterization and clinical validation of photoacoustic imaging.

Marcel C.M. Rutten received a M.Sc. degree in mechanical engineering from the Eindhoven University of Technology (TU/e), Eindhoven, The Netherlands, in 1993, and the Ph.D. degree from the Department of Mechanical Engineering, TU/e, in 1998, with a focus on fluid structure interaction in large arteries. Since 1998, he has been teaching cardiovascular mechanics with the Department of Biomedical Engineering, TU/e.

Patrick Bruneval is a Pathologist in Hôpital Européen Georges Pompidou, France.

Marc R.H.M. van Sambeek received the Medical degree from Catholic University, Nijmegen, The Netherlands, in 1986. He was a Surgeon with the Erasmus Medical Center, St. Francis Hospital, Rotterdam, The Netherlands, where he was a Staff Surgeon in 2007. He is currently a Vascular Surgeon at the Catharina Hospital, Eindhoven, The Netherlands. His special focus is on minimally invasive vascular surgery and endovascular treatment.

Frans N. van de Vosse studied applied physics at Eindhoven University of Technology from 1976 to 1982. He received a Ph.D. degree in 1987 with his study on the numerical analysis of carotid artery flow. He is a Professor with the Cardiovascular Biomechanics Group, Eindhoven University of Technology. His current research interests are related to the computational and experimental biomechanical analysis of the cardiovascular system and its application to clinical diagnosis and intervention, cardiovascular prostheses, extra corporeal systems, and medical devices.

Richard G.P. Lopata received the B.Sc. and M.Sc. degrees in biomedical engineering from the Eindhoven University of Technology (TU/e), Eindhoven, The Netherlands, and the Ph.D. degree from the Radboud University Nijmegen Medical Centre, Nijmegen, The Netherlands, with a focus on 3-D Functional Imaging of the Heart. He is currently an Associate Professor and head of the PULS/e Lab atg TU/e. His current research focuses on multimodality imaging, medical image analysis (strain imaging, elastography, 2-D and 3-D ultrasound, and photoacoustics) and image-based modeling in cardiovascular applications.